# Parallaxes of Southern Extremely Cool objects I: Targets, Proper motions and first results.

A.H. Andrei[1,2,3], R.L. Smart[2], J.L. Penna[1], V. A. d'Avila[1,4], B. Bucciarelli[2], J.I.B. Camargo[1], M. T. Crosta[2], M. Darpa[2], B. Goldman[5], H.R.A. Jones[6], M.G. Lattanzi[2], L. Nicastro[7], D.N. da Silva Neto[8] and R. Teixeira[9]

## ABSTRACT

We present results from the PARallaxes of Southern Extremely Cool objects (PARSEC) program, an observational program begun in April 2007 to determine parallaxes for 122 L and 28 T southern hemisphere dwarfs using the Wide Field Imager on the ESO 2.2m telescope. The results presented here include parallaxes of 10 targets from observations over 18 months and a first version proper motion catalog.

The proper motions were obtained by combining PARSEC observations astrometrically reduced with respect to the Second US Naval Observatory CCD Astrograph Catalog, and the Two Micron All Sky Survey Point Source Catalogue. The resulting median proper motion precision is 5mas/yr for 195,700 sources. The 140 0.3deg$^2$ fields sample the southern hemisphere in an unbiased fashion with the exception of the galactic plane due to the small number of targets in that region. The proper motion distributions are shown to be statistically well behaved. External comparisons are also fully consistent. We will continue to update this catalog until the end of the program and we plan to improve it including also observations from the GSC2.3 database.

We present preliminary parallaxes with a 4.2 mas median precision for 10 brown dwarfs, 2 of which are within 10pc. These increase by 20% the present number of L dwarfs with published parallaxes. Of the 10 targets, 7 have been previously discussed in the literature: two were thought to be binary but the PARSEC observations show them to be single, one has been confirmed as a binary companion and another has been found to be part of a binary system, both of which will make good benchmark systems. These results confirm that the foreseen precision of PARSEC can be achieved and that the large field of view will allow us to identify wide binary systems.

Observations for the PARSEC program will end in early 2011 providing 3-4 years of coverage for all targets. The main expected outputs are: more than a 100% increase of the number of L dwarfs with parallaxes; to increment - in conjuction with published results - to at least 10 the number of objects per spectral subclass up to L9, and; to put sensible limits on the general binary fraction of brown dwarfs. We aim to contribute significantly to the understanding of the faint end of the H-R diagram and of the L/T transition region.

*Subject headings:* Astrometry – Stars: low-mass, fundamental parameters, distances, proper motions

[1]Observatório Nacional/MCT, R. Gal. José Cristino 77, CEP20921-400, RJ, Brasil.

[2] INAF/Osservatório Astronomico di Torino, Strada Osservatório 20, 10025 Pino Torinese, Italy

[3] Observatório do Valongo/UFRJ, Ladeira Pedro Antônio 43, CEP20080-090, RJ, Brasil

[4] UERJ, Faculdade de Oceanografia, R. São Francisco Xavier 524, CEP20550-900, RJ, Brasil

[5]Max Planck Institute for Astronomy, Koenigstuhl 17, D–69117 Heidelberg, Germany

[6] Centre for Astrophysics Research, Science and Technology Research Institute, University of Hertfordshire, Hatfield AL10 9AB

[7]INAF/Istituto di Astrofisica Spaziale e Fisica Cosmica, Bologna, Via Gobetti 101, 40129 Bologna, Italy

[8] Centro Universitário Estadual da Zona Oeste, Av. Manuel Caldeira de Alvarenga 1203, CEP23070-200, RJ,

## 1. Introduction

The first brown dwarf, GD 165B, was discovered in 1988 (Becklin & Zuckerman) but was not recognised as such until 1995 when Gl229B (Nakajima et al.) and other objects with the same characteristics were found. Rapidly many examples were discovered primarily in the large infrared surveys, i.e. the Two Micron All Sky Survey (2MASS, Skrutskie et al. 2006) and Deep Near-Infrared Survey (DENIS, Epchtein et al. 1999), and, the deep optical Sloan Digital Sky Survey (SDSS, York et al. 2000). It was soon realized that new spectral types, L and T, were needed (Kirkpatrick et al. 1999). Since then over 700 L/T dwarfs have been discovered (www.dwarfarchives.org 2/2010) by various authors and just recently a sample of 210 new L dwarfs from the SDSS was announced (Schmidt et al. 2010). These objects have heralded a whole new sub-field of astronomy.

Interest in brown dwarfs has been particularly prominent in the interpretation of their spectral and photometric properties. Theory has been led in unexpected directions by unpredicted behaviors: the very strong evolution of spectral type with age (Burrows et al. 1997); the "hump" in the J band magnitude as a function of spectral type at the L/T transition (Tinney et al. 2003); notable differences between infrared spectra of optically classified objects and vice-versa (e.g. fig 3 in Kirkpatrick 2008); a turnaround in color at the T8/T9 spectral type (Warren et al. 2007). We are also slowly uncovering significant numbers of L and T sub-dwarfs (Sivarani et al. 2009; Burgasser 2004; Bowler et al. 2009, 2010) and other peculiar objects that challenge the theoretical models.

Parallax is a crucial parameter for understanding these objects as it is the only direct way to calculate an absolute magnitude and hence energetic output. In brown dwarf structure models, particularly for T dwarfs, the determination of metallicity and surface gravity from spectra is degenerate (Leggett et al. 2009) and hence luminosity, which requires a parallax, is used to constrain either the radius or the temperature and help break this degeneracy. Precise absolute velocities, that in turn provide age and origin indications, require precise parallaxes.

In light of the role of distance it is important that for these new objects we have a significant sample with measured parallaxes. As shown in Figure 1, only a small fraction of known L/T dwarfs have measured parallaxes - the black histogram - which limits any calibrations and generalizations we can make. To increase the current sample the Osservatorio Astronomico of Turin and Observatório Nacional of Brazil begin in 2007 the PARarallaxes of Southern Extremely Cool objects (hereafter PARSEC) program to determine parallaxes for 140 bright L and T dwarfs. In Figure 1 we include the PARSEC objects that illustrate our goal to attain at least 10 objects per spectral bin for L dwarfs and to increase the current sample for the fainter T dwarfs. A number of other programs are also underway to address this shortfall (for example C. G. Tinney private communication and J. K. Faherty as part of the Brown Dwarf Kinematics Project (Faherty et al. 2009)) but even including the expected additional objects the results of the PARSEC program will at least double number of L and bright T dwarfs with parallaxes.

In this paper we present the PARSEC program: section 2 describes the instrument and target selection; section 3 details the observational and reduction procedures, and section 4 the procedures used to produce a catalog of standard proper motions and preliminary parallax solutions for 10 objects. Finally in section 5 we discuss some uses we have made of this catalog and future plans.

## 2. The PARSEC observational program

### 2.1. The instrument

The primary instrument for this program is the Wide Field Imager (WFI, Baade et al. 1999) on the ESO 2.2m telescope. This is a mosaic of 8 EEV CCD44 chips with 2k×4k 15 $\mu$m pixels, providing a total field of 32.5 by 32.5 arcmin. This instrument/telescope combination was chosen for a number of reasons:

1. The instrument is fixed and stable, both crucial requirements in relative astrometry work
2. The plate scale of 0.2"/pixel is optimal for this work as it offers better than Nyquist sampling even in the best seeing.

Brasil

[9]Instituto de Astronomia, Geofsica e Cincias Atmosfricas, Universidade de So Paulo, Rua do Mato, 1226 - Cidade Universitria, 05508-900 So Paulo - SP, Brazil

3. The field size of 0.3 square degrees allows a reasonably thorough search for nearby companions

4. It already has a proven track record for the determination of parallaxes of dwarf objects (Ducourant et al. 2007)

It was decided to observe in the $z$ band (Z+/61 ESO#846, central wavelength 964.8nm, FWHM 61.6nm) which was a compromise between the optimal QE of the system in the $I$ band, and the expected brightness of the targets which have a $I-z$ of about 2. To keep the exposure times within 300s we observed only objects brighter than $z$ <19.

### 2.2. Observations

The observational procedure is as follows.

1. For each field we make one quick 50s exposure and locate the target.

2. Using the WFI move-to-pixel procedure we offset the telescope to move the target to pixel (3400,3500), which is in a flat part of CCD#7 (Priscilla) at less than 1/4 of the diagonal leading to the optical center of the mosaic.

3. We make the first science exposure of 150s for objects with $z$ <18.0 and 300s for $z \geq$18.0.

4. The camera is then slightly offset, 24 pixels in both directions, and the second science image of the same exposure time is automatically begun.

5. We check the counts of the target in the first image. If the signal-to-noise of the target in the first image is less than 100, in real time we increased the exposure time accordingly. This is usually only the case in particularly poor sky conditions.

This procedure is very efficient and the dead-time for the telescope is minimal. The total time for a target is 10-25 minutes depending on magnitude and other overheads, enabling us to observe 3-4 objects per hour. Our time allocation usually results in always having grouped nights and, as multiple observations in the same run are of limited value, to both increase the sample and allow some redundancy, the target list has 6-8 objects per hour. We attempted to observe the majority of targets close to the meridian except during the twilight hours when we wish to include rising or setting targets at their maximum parallactic factor.

Observations began in April 2007 and, as of September 2009, targets have between 1.5 and 2.5 years of observations. The frequency of observations have been reasonably constant with a 2-3 night run every two months.

Figure 2 displays the sky distribution of the targets. Table 1 summarizes the dates and nights of the observations taken up 2009.

Table 1: Observations of the PARSEC program at the ESO2p2/WFI up to 2009.

| Date | Nights |
|---|---|
| April 2007 | 09, 10, 11, 12 |
| August 2007 | 31 |
| September 2007 | 01, 02 |
| October 2007 | 05, 06, 07 |
| January 2008 | 04, 05 |
| February 2008 | 26, 27 |
| April 2008 | 02, 03 |
| May 2008 | 27, 28 |
| August 2008 | 21, 22 |
| October 2008 | 24, 26 |
| December 2008 | 18, 20 |
| March 2009 | 01, 02, 03 |
| April 2009 | 30 |
| May 2009 | 06, 08 |
| July 2009 | 21, 22, 23 |
| December 2009 | 15, 18, 21 |

### 2.3. Target Selection

The targets were selected using the following criteria:

1. All southern L and T dwarfs discovered before April 2007

2. Brighter than $z$=19

3. No more than 8 objects in any RA hour

4. The brightest examples within each spectral bin

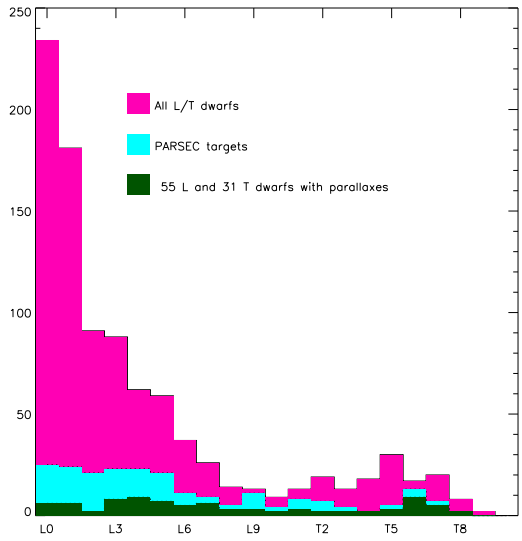


Fig. 1.— The distribution of the 752 known L and T dwarfs as of 2/2010 (www.dwarfarchives.org). Overplotted the distribution of the 90 objects with published parallaxes and the 140 objects in the PARSEC program as indicated in the legend.

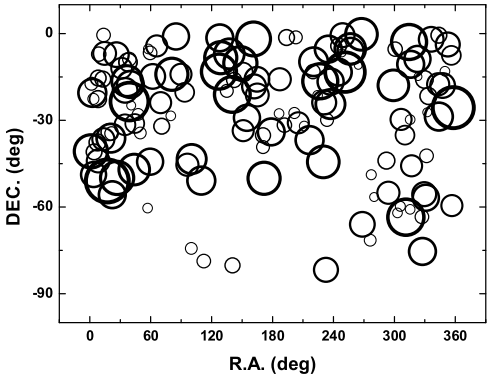


Fig. 2.— The equatorial coordinates distribution of the 140 sources of program. The size of the circles is in proportion to the object $z$ magnitude. Notice that all targets belong in the austral hemisphere, and that they are clear of the galactic disk.

5. A uniform spectral class distribution

6. A photometric distance smaller than 50pcs.

The photometric distances were estimated using the 2MASS magnitudes transformed to the MKO system using Stephens & Leggett (2004) and the color - absolute magnitude compilation given in Knapp et al. (2004). Exceptions were made to include any objects that were underrepresented, e.g. most known T dwarfs are too faint for this program so any T dwarf with z $<$ 19 was given high priority. By applying the above criteria and by removing those objects we were not able to observe during the first runs due to time compression, the remaining list has 140 targets as shown in table 2. Listed are: the 2MASS counterpart name, shortened name used in this paper, published $z$-band magnitude - if no published value is available this is estimated from the J band magnitude and spectral type, 2MASS magnitudes, nominal spectral type and the discovery name. Most of the objects were chosen from the dwarfarchives.org while some are from the catalogs of Deacon & Hambly (2007) and Pokorny et al. (2004).

### 2.4. Image Reduction Procedures

The bias, dark and flat image corrections followed standard procedures while fringe removal required a tailored approach. The interference fringes in the WFI $z$-band image are severe, an examination of the counts shows they can vary by up to 10% over the distance of a few pixels. Fringing is an additive effect that can be corrected making a fringe map and subtracting it from the raw images. The suggested WFI approach is to apply a standard fringe map which is updated at periodic intervals. We found it improved our centroiding by adopting a different approach and to understand why we first consider the cause of fringing.

Fringes are caused by the constructive and destructive interference of the night sky emission lines that are reflected from the bottom of the CCD silicon layer with incoming radiation. Fringes are time and observation dependent for a number of reasons e.g.: changes in the brightness of the night sky emission lines, changes in the thickness of the silicon layer which is a function of the temperature of the CCD, changes in the angle of incidence of the light on the CCD which is a function of flexure. The ideal case would therefore

be to make a fringe map for each image but this is not feasible. Our compromise is to make a nightly fringe map whenever possible.

The general procedure to construct a fringe map is to mask out objects then build a mean map from all of the observations in a given night scaled appropriately to reveal the fringe signal. Specifically we followed the following steps:

1. For all images we identify all the objects and make an object mask.

2. For each image we make a sky map by fitting a plane to all the unmasked pixels including a $3\sigma$ clipping rejection criteria. This changes in the course of the night so it is necessary to remove it from each frame independently.

3. We select a fringe calibration image subset consisting of all the short 50s and 4 of the long science exposures. We did not include all the science images in this subset as the object mask does not always cleanly block out all of the target signal and using all the science frames with the target on the same pixel results in a ghost image around the move-to-pixel position.

4. We make a median image by scaling all subset images by the exposure time and making a median of the unmasked pixels.

5. The first fringe map is constructed by smoothing the median image using a block size of 5 pixels.

6. This first fringe is subtracted from all images providing sky subtracted and relatively fringe free observations.

7. We make a new median image scaling the cleaned subset images by the weighted mean difference between the input image and the fringe image.

8. We construct a new fringe map smoothing the median image and then apply it to all the cleaned images providing fringe-free images.

In the first iteration we use the exposure time as a scale factor as the fringing will systematically affect the mean image counts, in the second the majority of the fringes are removed and we use the mean count as the scale factor which reflects the overall sky conditions as well. Below we discuss the effect of this fringing on the centroiding.

### 2.5. Centroiding and Feasibility Tests

The WFI, having a large field of view, has significant astrometric distortions and the CCDs have significant relative tilts (see the WFI section at www.eso.org). However, the fundamental requirements for relative astrometry, that underlie **all** small field parallax determinations, are stability and repeatability. For this reason we use the WFI move-to-pixel routine to put the target on the same pixel for each science exposure and only consider astrometric distortion changes over the observational campaign. The move-to-pixel position, (3400,3500), is sufficiently inside CCD#7 that reference stars from only the top third of the chip are needed to make a low-noise astrometric transformation between different epochs. The move-to-pixel procedure introduces a significant overhead but as shown by Platais et al. (2002), on a similar mosaic, the chips move relative to one another and this introduces a change in the astrometric deformation that was impossible to model at the mas level as required by our parallax goal.

We have tested three centroiding routines: a two dimensional Gaussian fit to the psf as used in the Torino Observatory Parallax Program (Smart et al. 1999, TOPP), a one-dimensional Gaussian fit to the marginal distributions, and the Gaussian psf fit provided by daophot in IRAF. In a comparison of object positions observed on 14 nights over an 18-month period of the field around the object 0719-50 we found the TOPP routine worked best. In figure 3 we plot rms of the position differences as a function of instrumental $z$ magnitude for the frames in question. The median rms for all objects is 23mas and for the brighter objects from 12-16 is 10mas. If we apply the same test on images that have not been fringe-corrected as described above we find the median precision has deteriorated to 28mas. Applying the fringe map supplied by the WFI calibration team provided a precision that was intermediate between a nightly fringe correction and no correction.

Table 3: Parallaxes and proper motions for a sample of PARSEC L-dwarfs.

| ID | $\alpha$ h:m:s | $\delta$ d:':" | $N_*, N_f$ | $\pi$ mas | $\mu_\alpha$ mas/yr | $\mu_\delta$ mas/yr | $\Delta$T yrs | COR mas |
|---|---|---|---|---|---|---|---|---|
| 0539-00 | 5:39:51.9 | - 0:58:58.3 | 31, 12 | 82.0 ± 3.1 | 157.0 ± 4.8 | 321.6 ± 3.9 | 1.40 | 1.13 |
| 0641-43 | 6:41:18.5 | -43:22:28.0 | 14, 29 | 55.7 ± 5.7 | 215.9 ± 8.9 | 612.8 ± 9.0 | 1.95 | 1.00 |
| 0719-50 | 7:19:32.0 | -50:51:41.3 | 22, 34 | 32.6 ± 2.4 | 198.1 ± 3.2 | -61.4 ± 3.9 | 1.98 | 0.90 |
| 0835-08 | 8:35:42.2 | - 8:19:21.7 | 9, 20 | 117.3 ± 11.2 | -519.8 ± 7.7 | 285.4 ± 10.5 | 1.96 | 1.08 |
| 0909-06 | 9:09:57.3 | - 6:58:18.8 | 20, 23 | 42.5 ± 4.2 | -184.0 ± 2.5 | 20.7 ± 3.0 | 2.08 | 1.19 |
| 1004-33 | 10:04:39.5 | -33:35:21.9 | 16, 22 | 54.8 ± 5.6 | 243.5 ± 4.0 | -253.2 ± 3.4 | 2.06 | 9.51 |
| 1018-29 | 10:18:58.5 | -29:09:54.2 | 32, 23 | 35.3 ± 3.2 | -340.8 ± 1.8 | -94.0 ± 2.7 | 2.08 | 1.01 |
| 1539-05 | 15:39:42.1 | - 5:20:41.5 | 17, 18 | 64.5 ± 3.4 | 603.1 ± 2.6 | 105.0 ± 3.4 | 2.06 | 1.12 |
| 1705-05 | 17:05:48.4 | - 5:16:46.9 | 96, 17 | 44.5 ± 12.0 | 110.9 ± 12.1 | -115.5 ± 7.1 | 1.98 | 0.59 |
| 1750-00 | 17:50:24.5 | - 0:16:13.6 | 29, 39 | 108.5 ± 2.6 | -398.3 ± 3.1 | 195.3 ± 3.4 | 2.08 | 0.56 |

NOTE.—$N_*$ = number of reference stars, $N_f$ = number of frames, $\Delta$T = epoch range, COR = correction to absolute parallax.

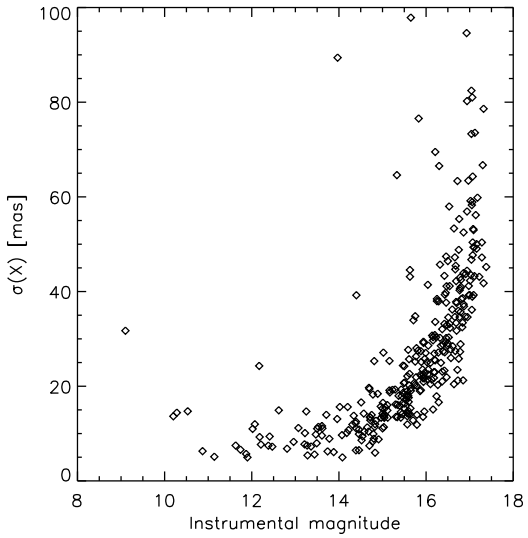


Fig. 3.— The root-mean-square of the X coordinates residuals for stars in common with a 0719-50 image sequence spanning 1.5 years as a function of $z$ magnitude. The centroids were all derived using the TOPP two dimensional gaussian fit.

## 3. Parallaxes

To determine parallaxes for our targets we consider only the top third of CCD#7. This is sufficiently large that, at these magnitudes, we have enough reference objects for a transformation to a common system and sufficiently small we can assume the variation in astrometric distortion over the observational campaign is smaller than the errors of a linear transformation. Once the (x,y) coordinates have been determined, the parallax and proper motions are derived using the methods adopted in TOPP (Smart et al. 2003, 2007). Schematically, we transfer the base frame to a standard coordinate system using the UCAC2 stars, adjust all subsequent frames to this base frame using all common stars and a simple linear transformation, and find the relative parallax and proper motion of the target star by a fit to the resulting observations in the system of the base frame. In the $z$-band the atmospheric refraction is small and we assume the differential color refraction to be negligible (Stone 2002). To calculate the correction from relative to absolute parallax we use the galaxy model of Mendez & van Altena (1996) in the $z$ band to estimate the mean distance of the common stars. For the reference stars in these fields this parallactic mean distance

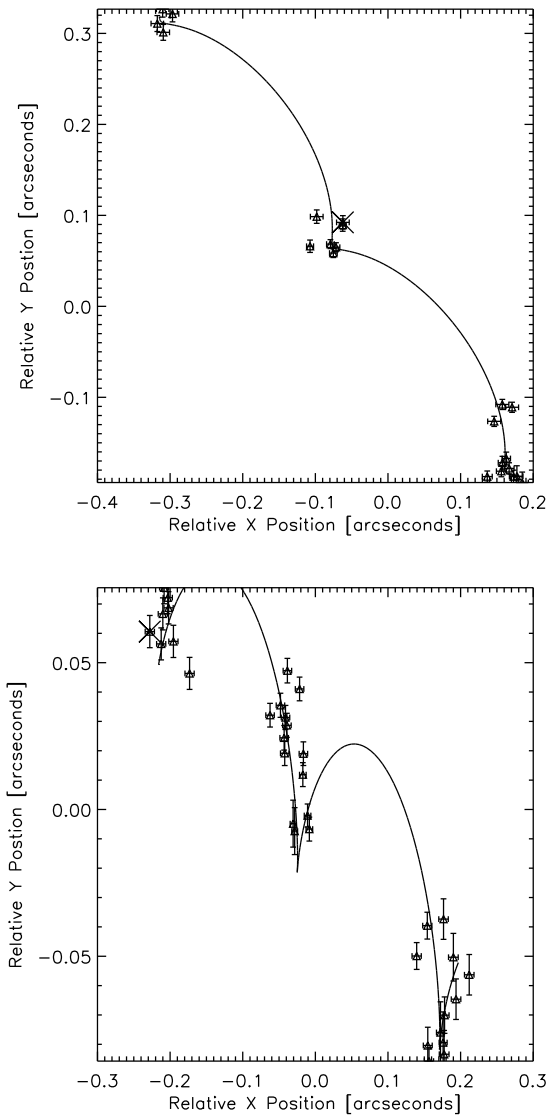


Fig. 4.— Observations for two example targets 0719-50 and 1004-33.

is of the order of 1mas with an error of <30% . For more details on the parallax determination procedure and this correction the reader is refered to Smart et al. (2003, 2007).

In figure 4 we reproduce the solutions for two targets, 0719-50 and 1004-33. These two objects were also found to have companions as discussed below. In Table 3 we report the parallaxes for 10 objects observed in the early runs of the PARSEC program. Listed are: object ID, position, number of stars, number of frames, absolute parallax, absolute proper motions, epoch difference and correction applied from relative to absolute parallax. In the following we discuss some of these objects in more detail.

*0539-00* This object was found to have a photometric variability on a timescale of 13.3h (Bailer-Jones & Mundt 2001), we note in our sequence the instrumental magnitude decreases by 0.05±0.03 magnitudes over the two year sequence. The radial velocity was found not to vary for two observations spaced 4 years, excluding a companion of mass greater than 10 $M_J$ (Zapatero Osorio et al. 2007); the astrometric residuals also show no evidence for binarity.

*0719-50* For this object we find $\mu_\alpha, \mu_\delta$ = 198.1 ± 3.2, -61.4 ± 3.9 mas/yr and it is identified by the PARSEC observations as a common proper motion companion of 2MASS07193535-5050523 with $\mu_\alpha, \mu_\delta$ = (200.3 ± 8.9, -67.6 ± 5.7). The parallaxes both agree within the errors confirming the binary nature of this system. Both these objects have previous proper motion estimates, 0719-05 of 199.11 ± 20.49, -46.440 ±13.78 mas/yr (Casewell et al. 2008) and 2MASS07193535-5050523 of 206.2,-64.2 (Finch et al. 2007), but they were not noted as a common proper motion system. The analysis of the proper motion distributions in the range of magnitude and in the sky loci surveyed by the entire PARSEC program, gives a probability smaller than 0.002 for a chance occurance of such common pair of large proper motions. This chance becomes even smaller if the common distance is also considered. The brighter star has GSC2.3 magnitudes of $B_J$ =16.01, $R_f$ =13.50 and $I_n$=11.60 and 2MASS magnitudes of $J$=10.33, $H$=9.74, and $K$= 9.482. Combining the magnitudes and distance with the calibrations in Hawley et al. (2002) we find that the most consistent spectral type for this object is a M3-M4 dwarf.

*0835-08* Cruz et al. (2003) find a spectroscopic distance of 8.3pc in agreement with our distance of 8.5pc, the nearest target in this sample and one of nearest known L dwarfs to date. The astrometric residuals present no evidence of binarity, which, combined with the consistency of the photometric and parallactic distances, allows us to confidently say that this is a single system.

*0909-06* This is considered the prototypical L0 object, marking the begining of the L dwarf sequence with a temperature of 2200K (Basri et al. 2000). We expect by the end of the program to have the distance to this object to better than 5%.

*1004-33* We confirm, as suggested in Casewell et al. (2008) and Seifahrt et al. (2005), that this object is a binary companion of the nearby bright object LHS5166. The proper motions and parallaxes of the two objects are both within one sigma of each other. The brighter star has GSC2.3 magnitudes of $B_J$ =15.51, $R_f$ =13.33 and $I_n$=11.29 and 2MASS magnitudes of $J$=9.85, $H$=9.30, and $K$=9.03. Combining the magnitudes and distance with the calibrations in Hawley et al. (2002) we find the spectral type for this object is a M3 dwarf consistent with the dM4.5e found in Seifahrt et al. (2005).

*1705-05* In Reid et al. (2006) they consider the possibility that this object is part of a binary system with a companion at position angle of 5° and distance 1".36. This proposed companion was too faint to be frequently observed as part of our program, however, the color indicates a spectral type of T1-T2 that is inconsistent with the spectral type indicated by the apparent magnitude and distance of T7-T9. Hence, we conclude this object is more likely to be a background late M dwarf at ∼200 parsecs rather than a companion to 1705-05.

*1750-00* Based on spectroscopic observations, Kendall et al. (2007) found a distances of $8^{+0.9}_{-0.8}$pc and due to a discrepancies in the spectral type indicators suggest that it may be a binary system of L5-L6 and L8-L9 dwarfs. We find the trigonometric distance is consistent with the photometric one and do not find any evidence of binarity in the residuals which implies it is a single system and the discrepancies must have some other explanation.

*0641-43, 1018-29* & *1539-05* The first two objects are type L1, and the third is L2. They are all in the 20-30pc distance range. 0641-43 and 1539-05 are fast moving objects, with one of the proper motion components larger than 600mas/yr. None of them was the subject of any particular discussion in the literature.

Figure 5 compares the trigonometric parallaxes from Table 3 against the corresponding spectroscopic parallaxes based on the calibration of Knapp et al. (2004). The small number of sources precludes any direct conclusion, yet the targets asymmetry relatively to the equal values diagonal brings support to the importance of trigonometric parallaxes as the fundamental calibrators for spectroscopic distances.

## 4. Proper Motions

The parallax determination of the targets uses only the upper third of CCD7; however, the reduction pipeline is applied to the entire mosaic of 8 CCDs. From this data we have constructed a proper motion catalogue, sampling the whole of the southern hemisphere with the exception of the lowest galactic latitudes where the number of known L/T dwarfs is significantly reduced. This proper motion survey can be used to search for companions to the targets, and other fast moving objects which will usually be nearby and/or sub-dwarfs. Combined with the magnitudes, the proper motion survey can also be used to build a reduced proper motion diagram to search for brown dwarf candidates. This catalog contains proper motion determinations for 195,700 objects.

Independently for each CCD and each observation we have determined an astrometric reduction relative to the Second US Naval Observatory CCD Astrograph Catalog (UCAC2, Zacharias et al. 2004). The average number of reference stars was 20, with which polynomial functions were adjusted on right ascension and declination. Depending on the number of reference stars the polynomial degree was 2 or 3 and cross terms have been included. The rms errors of the solutions did not show any dependence on the type of polynomial employed.

The proper motion determination was made from a match to the 2MASS point source catalogue. In principle, the program frames should be complete with respect to 2MASS and the epoch difference is small, so a nearest neighbor match should be sufficient to not mismatch high proper

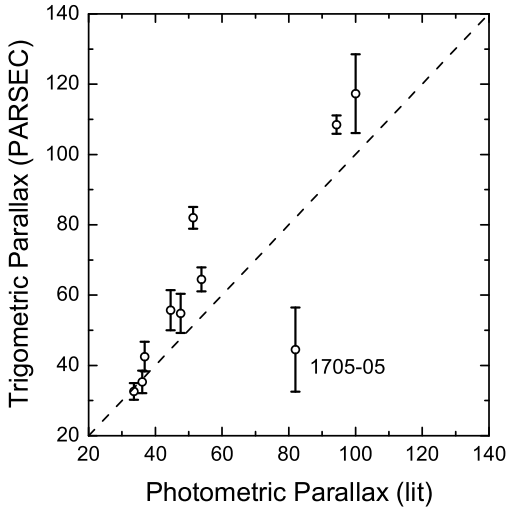


Fig. 5.— Comparison between the preliminary parallaxes derived by the PARSEC program for the 10 targets in Table 3 against the corresponding spectroscopic parallaxes. Notice how the photometric parallax of 1705-05 is affected by the superimposed nearby star (see text).

motion objects. As a safety measure, the proper motions were determined for each observation combination and later averaged. Deviant values were removed from these averages, as they either came from unrecognised frame defects or faulty measurements. A more robust algorithm is being developed using the GSC2.3 positions at different epochs. At the targets galactic latitudes, blending is rare and its effects would be negligible to the relatively bright 2MASS stars.

The histograms of the right ascension and declination proper motions distributions are presented in Figure 6. The mean value for $\alpha$ is -2.8mas/yr (standard deviation $\sigma$=12.1mas), and -4.0mas/yr (standard deviation $\sigma$=12.3mas) for $\delta$. This compares well with the corresponding values for the UCAC2 catalogue in the same regions, which are, -2.7mas/yr (standard deviation $\sigma$=14.6mas) for $\alpha$, and -3.6mas/yr (standard deviation $\sigma$=30.1mas) for $\delta$. Zonal averages ($3^h \times 30°$) also produced similar means for the PARSEC program and the UCAC2 catalogue stars. Figure 7 compares the proper motions of stars in common with the PARSEC program and the UCAC2 catalogue. The Pearson's linear correlation coefficient is 0.95 both on right ascension and on declination. The largest difference appear for the smallest proper motions ( 25mas/yr), the central parts in figure 7, where the PARSEC values typically exceed those from the UCAC2 by 6%.

Figure 8 is a similar comparison of the program target proper motions against values found in the literature. The linear correlation is 0.82. There are 5 outliers: 0523-14, 0559-14, 0624-45, 1828-48, and 1956-17. For each of the outliers a local comparison against the UCAC2 proper motions within the target's CCD have shown the same level of agreement found for the program as a whole. In the case of 0523-14 and 0624-45 the original proper motion paper (Schmidt et al. 2007) does not have any special discussion of these sources. Our results come respectively from 2 and 3 PARSEC observations, and more data must be added on to reach a clearer understanding. For 0559-14, the original proper motion paper (Dahn et al. 2002) indicates that the proper motion was taken within just 2.1 years, and the results should be taken as preliminary. For 1828-48 the original proper motion paper (Burgasser et al. 2004) indicates troublesome observations at high air mass and under

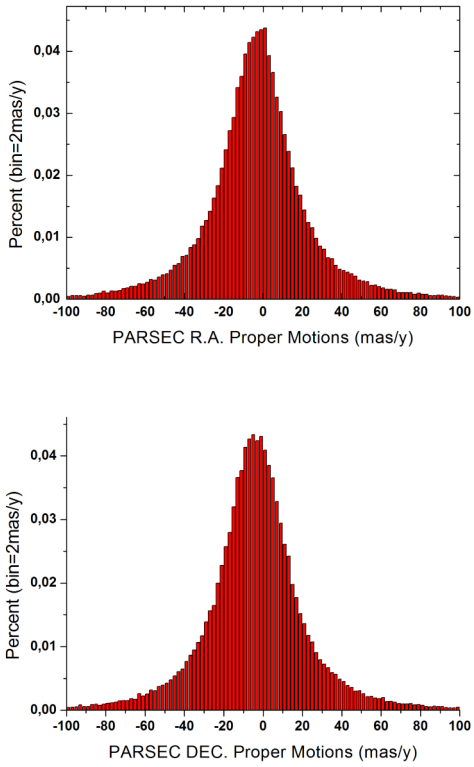


Fig. 6.— Proper motion distributions in right ascension and declination.

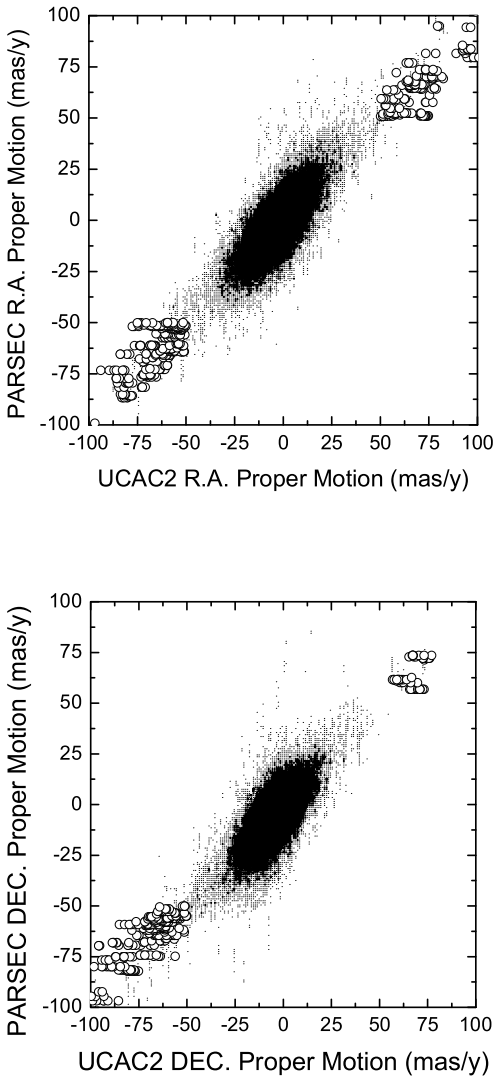


Fig. 7.— Comparison to UCAC2 proper motions in Right Ascension top panel and in Declination lower panel. For the smaller proper motions, the pairs in bins of 1mas/y are represented by dots with sizes proportional to the counts in the bin. The pairs in which any member is larger than |50|mas/y are individually represented by open circles.

patchy skies. For 1956-17 the original proper motion paper is from the SuperCOSMOS Sky Survey (Hambly et al. 2001) which for individual objects may have large errors while our results include 7 consistent PARSEC observations.

The histograms of the proper motion errors are shown in Figure 9. The mean values are 5mas/yr both for right ascension and declination. The similarity of the behaviour in both coordinates, already seen in the comparison to UCAC2 values and for the errors distribution, is shown in Figure 10, where the pair-wise RA and DEC proper motions are plotted for all objects. The actual proper motions distribution reflects several factors, prominently the galactic rotation, and an uniform distrubution modulated by the inverse square of the distance. The combination of factors may result either in a Poisson-like or in a Gaussian-like distribution. We want to investigate whether the peculiar geometry of each CCD, and/or some artifact left by the astrometric reduction made indepently for each of them would reflect on the proper motions distribution. In order to not assume an a priori model, the cumulative density distribution of the proper motions was fitted by an exponential decay, either along the RA or the DEC directions, and indeed when those are quadratically combined to produce the apparent sky motion. The exponential decays are characterized by the one free parameter which we call scale length. It is an uncomplicated, robust estimator borrowed from the description of stochastic processes in which events can occur continuously and are independently of one another. We calculated the scale length in density steps of 10mas/yr in order to investigate the presence of clumps, voids, or systematics within the parent proper motions population. This was done for each CCD, as shown in Table 4. From one CCD to another the variation of the least-squares adjusted scale length was always smaller than the rms of the adjustments, implying consistent astrometric precision from the different CCDs.

The proper motion catalogue will be provided upon request ([1]). We have chosen not to distribute it to the data centers until the observations are finished and we have a final product. The above

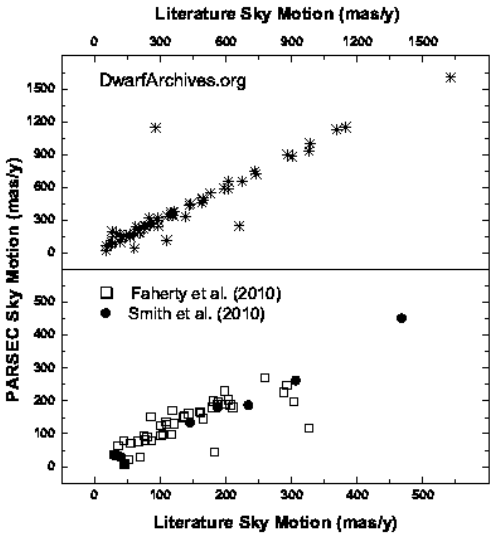


Fig. 8.— Comparison to literature values of the proper motions for the targets. On the top panel the comparison is made for the 58 PARSEC targets found in the archives of DwarfArchives.org. On the bottom panel the comparison is made for the most recent papers - 45 PARSEC targets in Faherty et al. (2010) and 8 PARSEC targets in Smith et al. (2010). Notice the different scale range in the two panels

[1]The preliminary catalog can be asked to the PARSEC team through oat1@on.br.

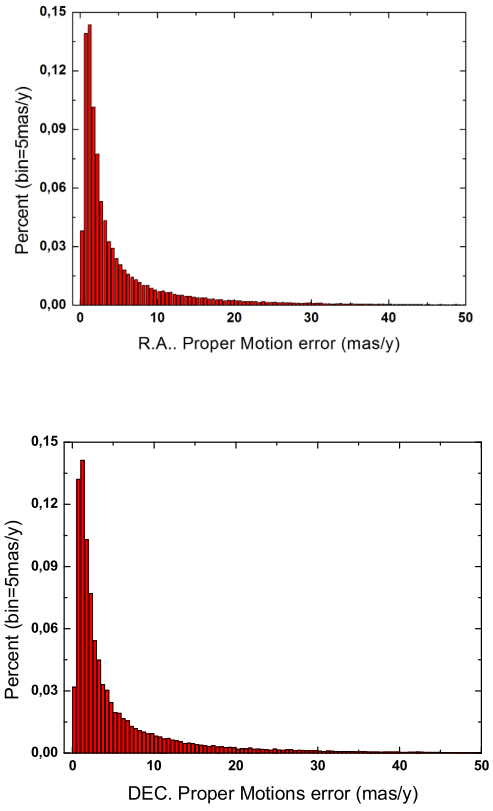


Fig. 9.— The distribution of the right ascension and declination proper motion errors.

Table 4: Scale length of the exponential decay of the separate and total proper motion distributions. Values are presented for all objects, and then by CCD.

| CCD | Scale Length | | |
|---|---|---|---|
| | Total +/- $\sigma$ mas/yr | $\mu_\alpha \pm \sigma$ mas/yr | $\mu_\delta \pm \sigma$ mas/yr |
| ALL | 34.3 ± 7.6 | 35.9 ± 8.0 | 34.4 ± 7.7 |
| 1 | 34.3 ± 7.6 | 35.9 ± 8.0 | 34.4 ± 7.7 |
| 2 | 30.7 ± 6.6 | 30.6 ± 7.1 | 29.0 ± 6.5 |
| 3 | 29.7 ± 6.3 | 29.6 ± 6.8 | 30.6 ± 6.7 |
| 4 | 35.9 ± 8.0 | 34.4 ± 7.7 | 34.1 ± 7.8 |
| 5 | 30.6 ± 7.1 | 29.0 ± 6.5 | 30.0 ± 6.9 |
| 6 | 29.6 ± 6.8 | 30.6 ± 6.7 | 26.6 ± 6.2 |
| 7 | 34.4 ± 7.7 | 34.1 ± 7.8 | 30.7 ± 7.3 |
| 8 | 29.0 ± 6.5 | 30.0 ± 6.9 | 27.0 ± 6.8 |

evaluation and our first release is based on the first year of the program, comprising 6 observation periods, from April/2007 up to April/2008.

In figure 11 we plot the reduced proper motion, $H(K) = K + 5 \times log(\mu_{tot}) + 5$, as a function of the $z - K$ color. The $z$ magnitudes come from a zero point correction to the instrumental magnitudes of the first observations, the $K$ are 2MASS magnitudes. The points are anonymous field stars and the diamonds are the brown dwarf targets. The line shows the cut we used to identify possible brown dwarf candidates for spectroscopic followup.

## 5. Conclusion

We have presented the first parallaxes from the PARSEC program. The results bode well for the whole program which is expected to finish in early 2011. We have confirmed a candidate binary (1004-33) and discovered another (0719-50), both of which will make good benchmark systems. The WFI has a large field of view so we are able to put very good constraints on the wide binary systems and the parallaxes allow us to immediately isolate unresolved binaries because of their over luminosity with respect to their color. Given these two properties, and the large sample, we expect to be able to put sensible constraints on the binary fraction of brown dwarfs, a quantity that is critical for

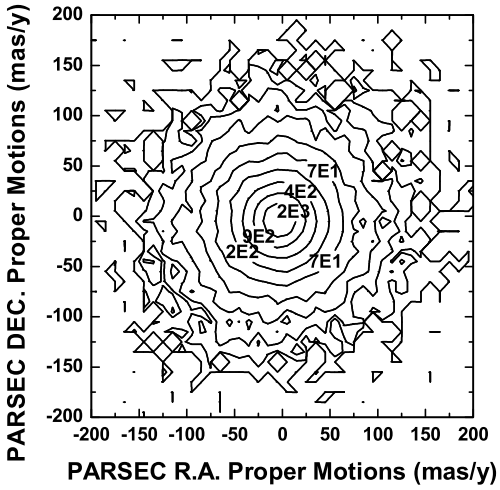


Fig. 10.— The right ascension vs declination proper motion contour plot for all the stars in the PARSEC fields.

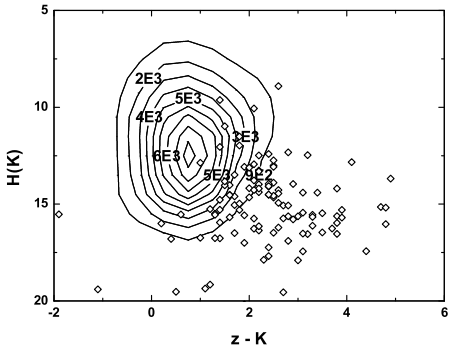


Fig. 11.— A reduced proper motion diagram of all objects in the PARSEC proper motion catalog. Diamonds are the targets and delineate the brown dwarf zone. The countour levels mark the quantity of field stars within the zone of the diagram. Fram the field stars furthermost in the tarfets zone possible brown dwarf candidates can be identified for spectroscopic followup.

estimating the substellar mass function. We have produced a catalog of proper motions sampling the whole of the southern hemisphere. This catalogue provides an independent validation of the UCAC2 proper motion system. The proper motion distributions are shown to be statistically well behaved, it follows that the proper motions for the fainter objects will have the same precision. We will continue to update online this catalog until the end of the program and we plan to improve it including also GSC23 database observations.

## 6. Acknowledgments

The authors would like to acknowledge the support of: the Royal Society International Joint Project 2007/R3; the PARSEC International Incoming Fellowship and IPERCOOL International Research Staff Exchange Scheme within the Marie Curie 7th European Community Framework Programme. AHA thanks CNPq grant PQ-307126/2006-0. JIBC acknowledges CNPq financial support #477943/2007-1. DNSN thanks FAPERJ grant E-26/110.177/2009.

This research has made use of: the SIMBAD database operated at CDS France; the Second Guide Star Catalog developed as a collaboration between the Space Telescope Science Institute and the Osservatorio Astronomico di Torino; the Two Micron All Sky Survey which is a joint project of the University of Massachusetts and the Infrared Processing and Analysis Center/California Institute of Technology; and, the M, L, and T dwarf compendium housed at dwarfArchives.org and maintained by Chris Gelino, Davy Kirkpatrick, and Adam Burgasser.

## REFERENCES

Baade, D., et al. 1999, The Messenger, 95, 15

Bailer-Jones, C. A. L., & Mundt, R. 2001, A&A, 367, 218

Basri, G., Mohanty, S., Allard, F., Hauschildt, P. H., Delfosse, X., Martín, E. L., Forveille, T., & Goldman, B. 2000, ApJ, 538, 363

Becklin, E. E., & Zuckerman, B. 1988, Nature, 336, 656

Bowler, B. P., Liu, M. C., & Cushing, M. C. 2009, ApJ, 706, 1114

Bowler, B. P., Liu, M. C., & Dupuy, T. J. 2010, ApJ, 710, 45

Burgasser, A. J. 2004, ApJ, 614, L73

Burgasser, A. J., McElwain, M. W., Kirkpatrick, J. D., Cruz, K. L., Tinney, C. G., & Reid, I. N. 2004, AJ, 127, 2856

Burrows, A., et al. 1997, ApJ, 491, 856

Casewell, S. L., Jameson, R. F., & Burleigh, M. R. 2008, MNRAS, 390, 1517

Cruz, K. L., Reid, I. N., Liebert, J., Kirkpatrick, J. D., & Lowrance, P. J. 2003, AJ, 126, 2421

Dahn, C. C., et al. 2002, AJ, 124, 1170

Deacon, N. R., & Hambly, N. C. 2007, A&A, 468, 163

Ducourant, C., Teixeira, R., Hambly, N. C., Oppenheimer, B. R., Hawkins, M. R. S., Rapaport, M., Modolo, J., & Lecampion, J. F. 2007, A&A, 470, 387

Epchtein, N., et al. 1999, A&A, 349, 236

Faherty, J. K., Burgasser, A. J., Cruz, K. L., Shara, M. M., Walter, F. M., & Gelino, C. R. 2009, AJ, 137, 1

Finch, C. T., Henry, T. J., Subasavage, J. P., Jao, W., & Hambly, N. C. 2007, AJ, 133, 2898

Hambly, N. C., et al. 2001, MNRAS, 326, 1279

Hawley, S. L., et al. 2002, AJ, 123, 3409

Kendall, T. R., Jones, H. R. A., Pinfield, D. J., Pokorny, R. S., Folkes, S., Weights, D., Jenkins, J. S., & Mauron, N. 2007, MNRAS, 374, 445

Kirkpatrick, J. D. 2008, in Astronomical Society of the Pacific Conference Series, Vol. 384, 14th Cambridge Workshop on Cool Stars, Stellar Systems, and the Sun, ed. G. van Belle, 85–+

Kirkpatrick, J. D., et al. 1999, ApJ, 519, 802

Knapp, G. R., et al. 2004, AJ, 127, 3553

Leggett, S. K., et al. 2009, ArXiv e-prints

Mendez, R. A., & van Altena, W. F. 1996, AJ, 112, 655

Nakajima, T., Oppenheimer, B. R., Kulkarni, S. R., Golimowski, D. A., Matthews, K., & Durrance, S. T. 1995, Nature, 378, 463

Platais, I., et al. 2002, AJ, 124, 601

Pokorny, R. S., Jones, H. R. A., Hambly, N. C., & Pinfield, D. J. 2004, A&A, 421, 763

Reid, I. N., Lewitus, E., Allen, P. R., Cruz, K. L., & Burgasser, A. J. 2006, AJ, 132, 891

Schmidt, S. J., Cruz, K. L., Bongiorno, B. J., Liebert, J., & Reid, I. N. 2007, AJ, 133, 2258

Schmidt, S. J., West, A. A., Burgasser, A. J., Bochanski, J. J., & Hawley, S. L. 2010, AJ, 139, 1045

Seifhart, A., Mugrauer, M., Wiese, M., Neuhäuser, R., & Guenther, E, W. 2005, AN, 326, 974

Sivarani, T., Lépine, S., Kembhavi, A. K., & Gupchup, J. 2009, ApJ, 694, L140

Skrutskie, M. F., et al. 2006, AJ, 131, 1163

Smart, R. L., Bucciarelli, B., Lattanzi, M. G., Massone, G., & Chiumiento, G. 1999, Astron. Astrophys., 348, 653

Smart, R. L., Lattanzi, M. G., Jahreiß, H., Bucciarelli, B., & Massone, G. 2007, A&A, 464, 787

Smart, R. L., et al. 2003, A&A, 404, 317

Stephens, D. C., & Leggett, S. K. 2004, PASP, 116, 9

Stone, R. C. 2002, PASP, 114, 1070

Tinney, C. G., Burgasser, A. J., & Kirkpatrick, J. D. 2003, AJ, 126, 975

Warren, S. J., et al. 2007, MNRAS, 381, 1400

York, D. G., et al. 2000, AJ, 120, 1579

Zacharias, N., Urban, S. E., Zacharias, M. I., Wycoff, G. L., Hall, D. M., Monet, D. G., & Rafferty, T. J. 2004, AJ, 127, 3043

Zapatero Osorio, M. R., Martín, E. L., Béjar, V. J. S., Bouy, H., Deshpande, R., & Wainscoat, R. J. 2007, ApJ, 666, 1205

This 2-column preprint was prepared with the AAS LaTeX macros v5.2.

TABLE 2
PARSEC TARGETS AS OF 1/2009

| 2MASS ID | Red. ID | z | J | H | $K_s$ | ST | Discovery ID |
|---|---|---|---|---|---|---|---|
| 00043484-4044058 | 0004-40 | 15.8 | 13.109 | 12.055 | 11.396 | L4.5 | GJ 1001B, LHS 102B |
| 00062050-1720506 | 0006-17 | 18.4 | 15.662 | 14.646 | 14.010 | L2.5 | 2MASSI J0006205-172051 |
| 00100009-2031122 | 0010-20 | 16.5 | 14.134 | 13.368 | 12.882 | L0.0 | 2MASS J00100009-2031122 |
| 00135779-2235200 | 0013-22 | 18.6 | 15.775 | 14.595 | 14.036 | L4.0 | 2MASSI J0013578-223520 |
| 00145575-4844171 | 0014-48 | 16.8 | 14.050 | 13.107 | 12.723 | L2.5 | 2MASS J00145575-4844171 |
| 00165953-4056541 | 0016-40 | 18.0 | 15.316 | 14.206 | 13.432 | L3.5 | 2MASS J00165953-4056541 |
| 00300625-3739483 | 0030-37 | 17.9 | 15.204 | 14.426 | 13.885 | L3.0 | DENIS-P J003006.2-373948 |
| 00325584-4405058 | 0032-44 | 17.1 | 14.776 | 13.857 | 13.269 | L0.0 | EROS-MP J0032-4405 |
| 00324308-2237272 | 0032-22 | 17.9 | 15.388 | 14.512 | 13.962 | L1.0 | 2MASSI J0032431-223727 |
| 00332386-1521309 | 0033-15 | 18.0 | 15.286 | 14.208 | 13.410 | L4.0 | 2MASS J00332386-1521309 |
| 00345684-0706013 | 0034-07 | 18.2 | 15.531 | 14.566 | 13.942 | L3.0 | 2MASSI J0034568-070601 |
| 00511078-1544169 | 0051-15 | 18.0 | 15.277 | 14.164 | 13.466 | L3.5 | 2MASSW J0051107-154417 |
| 00531899-3631102 | 0053-36 | 17.2 | 14.445 | 13.480 | 12.937 | L3.5 | 2MASS J00531899-3631102 |
| 00540655-0031018 | 0054-00 | 18.3 | 15.731 | 14.891 | 14.380 | L1.0 | SDSSp J005406.55-003101.8 |
| 00584253-0651239 | 0058-06 | 17.1 | 14.311 | 13.444 | 12.904 | L0.0 | SIPS0058-0651 |
| 01090150-5100494 | 0109-51 | 14.6 | 12.228 | 11.538 | 11.092 | L1.0 | SIPS0109-5100 |
| 01174748-3403258 | 0117-34 | 17.9 | 15.178 | 14.209 | 13.489 | L2.0 | 2MASSI J0117474-340325 |
| 01230050-3610306 | 0123-36 | 16.4 | 13.639 | 13.108 | 12.191 | L2.0 | 2MASSJ01230050-3610306 |
| 01253689-3435049 | 0125-34 | 18.3 | 15.522 | 14.474 | 13.898 | L2.0 | 2MASSI J0125369-343505 |
| 01282664-5545343 | 0128-55 | 16.6 | 13.775 | 12.916 | 12.336 | L2.0 | SIPS0128-5545 |
| 01443536-0716142 | 0144-07 | 16.9 | 14.191 | 13.008 | 12.268 | L5.0 | 2MASS J01443536-0716142 |
| 01473282-4954478 | 0147-49 | 15.8 | 13.058 | 12.366 | 11.916 | L2.0[a] | ... |
| 02052940-1159296 | 0205-11 | 17.4 | 14.587 | 13.568 | 12.998 | L5.5 | DENIS-P J0205.4-1159 |
| 02182913-3133230 | 0218-31 | 17.4 | 14.728 | 13.808 | 13.154 | L3.0 | 2MASSI J0218291-313322 |
| 02192807-1938416 | 0219-19 | 16.9 | 14.110 | 13.339 | 12.910 | L2.5 | SSSPM J0219-1939 |
| 02271036-1624479 | 0227-16 | 16.1 | 13.573 | 12.630 | 12.143 | L1.0 | 2MASS J02271036-1624479 |
| 02304498-0953050 | 0230-09 | 17.7 | 14.818 | 13.912 | 13.403 | T0.0[a] | ... |
| 02355993-2331205 | 0235-23 | 15.2 | 12.690 | 12.725 | 12.186 | L1.0 | GJ 1048B |
| 02354756-0849198 | 0235-08 | 18.3 | 15.571 | 14.812 | 14.191 | L2.0 | SDSS J023547.56-084919.8 |
| 02394245-1735471 | 0239-17 | 16.6 | 14.291 | 13.525 | 13.039 | L0.0 | SIPS0239-1735 |
| 02431371-2453298 | 0243-24 | 18.9 | 15.381 | 15.137 | 15.216 | T6.0 | 2MASSI J0243137-245329 |
| 02550357-4700509 | 0255-47 | 16.1 | 13.246 | 12.204 | 11.558 | L9.0 | DENIS-P J0255-4700 |
| 02572581-3105523 | 0257-31 | 17.6 | 14.672 | 13.518 | 12.876 | L8.0 | 2MASS J02572581-3105523 |
| 03101401-2756452 | 0310-27 | 18.5 | 15.795 | 14.662 | 13.959 | L5.0 | 2MASS J03101401-2756452 |
| 03185403-3421292 | 0318-34 | 18.5 | 15.569 | 14.346 | 13.507 | L7.0 | 2MASS J03185403-3421292 |
| 03480772-6022270 | 0348-60 | 18.8 | 15.318 | 15.559 | 15.602 | T7.0 | 2MASS J03480772-6022270 |
| 03504861-0518126 | 0350-05 | 18.8 | 16.327 | 15.525 | 15.125 | L1.0 | SDSS J035048.62-051812.8 |
| 03572695-4417305 | 0357-44 | 16.7 | 14.367 | 13.531 | 12.907 | L0.0 | DENIS-P J035726.9-441730 |
| 03572110-0641260 | 0357-06 | 18.3 | 15.953 | 15.060 | 14.599 | L0.0 | SDSS J035721.11-064126.0 |
| 04082905-1450334 | 0408-14 | 16.9 | 14.222 | 13.337 | 12.817 | L4.5 | 2MASSI J0408290-145033 |
| 04234858-0414035 | 0423-04 | 17.3 | 14.465 | 13.463 | 12.929 | L0.0 | SDSSp J042348.57-041403.5 |

TABLE 2—*Continued*

| 2MASS ID | Red. ID | z | J | H | $K_s$ | ST | Discovery ID |
|---|---|---|---|---|---|---|---|
| 04390101-2353083 | 0439-23 | 17.3 | 14.408 | 13.409 | 12.816 | L6.5 | 2MASSI J0439010-235308 |
| 04430581-3202090 | 0443-32 | 18.0 | 15.273 | 14.350 | 13.877 | L5.0 | 2MASSI J0443058-320209 |
| 05185995-2828372 | 0518-28 | 18.8 | 15.978 | 14.830 | 14.162 | L1.0 | 2MASS J05185995-2828372 |
| 05233822-1403022 | 0523-14 | 15.9 | 13.084 | 12.220 | 11.638 | L5.0 | 2MASSI J0523382-140302 |
| 05395200-0059019 | 0539-00 | 16.7 | 14.033 | 13.104 | 12.527 | L3.0 | SIPS0539-0059 |
| 05591914-1404488 | 0559-14 | 17.3 | 13.802 | 13.679 | 13.577 | T4.5 | 2MASS J05591914-1404488 |
| 06141196-2019181 | 0614-20 | 17.6 | 14.783 | 13.901 | 13.375 | L4.0 | SIPS0614-2019 |
| 06244595-4521548 | 0624-45 | 17.2 | 14.480 | 13.335 | 12.595 | L5.0 | 2MASS J06244595-4521548 |
| 06395596-7418446 | 0639-74 | 18.5 | 15.795 | 14.723 | 14.038 | L5.0 | 2MASS J06395596-7418446 |
| 06411840-4322329 | 0641-43 | 16.3 | 13.751 | 12.941 | 12.451 | L1.5 | 2MASS J06411840-4322329 |
| 07193188-5051410 | 0719-50 | 16.5 | 14.094 | 13.282 | 12.773 | L0.0 | 2MASS J07193188-5051410 |
| 07291084-7843358 | 0729-78 | 18.3 | 15.440 | 14.947 | 14.635 | L0.0[b] | 2_3367 |
| 08283419-1309198 | 0828-13 | 15.6 | 12.803 | 11.851 | 11.297 | L2.0 | SSSPM J0829-1309 |
| 08320451-0128360 | 0832-01 | 16.6 | 14.128 | 13.318 | 12.712 | L1.5 | 2MASSW J0832045-012835 |
| 08354256-0819237 | 0835-08 | 15.9 | 13.169 | 11.938 | 11.136 | L5.0 | 2MASSI J0835425-081923 |
| 08592547-1949268 | 0859-19 | 18.4 | 15.527 | 14.436 | 13.751 | L6.0 | 2MASSI J0859254-194926 |
| 09095749-0658186 | 0909-06 | 16.2 | 13.890 | 13.090 | 12.539 | L0.0 | DENIS-P J0909-0658 |
| 09211410-2104446 | 0921-21 | 15.5 | 12.779 | 12.152 | 11.690 | L4.5 | 2MASS J09211410-2104446 |
| 09221952-8010399 | 0922-80 | 18.1 | 15.276 | 14.285 | 13.681 | L2.0 | 2MASS J09221952-8010399 |
| 09283972-1603128 | 0928-16 | 18.1 | 15.322 | 14.292 | 13.615 | L2.0 | 2MASSW J0928397-160312 |
| 09532126-1014205 | 0953-10 | 15.8 | 13.469 | 12.644 | 12.142 | L0.0 | 2MASS J09532126-1014205 |
| 10044030-1318186 | 1004-13 | 17.6 | 14.685 | 13.883 | 13.357 | T0.0[a] | ... |
| 10043929-3335189 | 1004-33 | 17.3 | 14.480 | 13.490 | 12.924 | L4.0 | 2MASSW J1004392-333518 |
| 10185879-2909535 | 1018-29 | 16.7 | 14.213 | 13.418 | 12.796 | L1.0 | 2MASSW J1018588-290953 |
| 10452400-0149576 | 1045-01 | 15.7 | 13.160 | 12.352 | 11.780 | L1.0 | 2MASSI J1045240-014957 |
| 10473109-1815574 | 1047-18 | 17.0 | 14.199 | 13.423 | 12.891 | L2.5 | DENIS-P J1047-1815 |
| 10584787-1548172 | 1058-15 | 16.9 | 14.155 | 13.226 | 12.532 | L3.0 | DENIS-P J1058.7-1548 |
| 10595138-2113082 | 1059-21 | 17.1 | 14.556 | 13.754 | 13.210 | L1.0 | 2MASSI J1059513-211308 |
| 11220826-3512363 | 1122-35 | 18.1 | 15.019 | 14.358 | 14.383 | T2.0 | 2MASS J11220826-3512363 |
| 11223624-3916054 | 1122-39 | 18.4 | 15.705 | 14.682 | 13.875 | L3.0 | 2MASSW J1122362-391605 |
| 11263991-5003550 | 1126-50 | 15.9 | 13.997 | 13.284 | 12.829 | L6.5 | 2MASS J11263991-5003550 |
| 11544223-3400390 | 1154-34 | 16.6 | 14.195 | 13.331 | 12.851 | L0.0 | 2MASS J11544223-3400390 |
| 12255432-2739466 | 1225-27 | 18.8 | 15.260 | 15.098 | 15.073 | T6.0 | 2MASS J12255432-2739466 |
| 12281523-1547342 | 1228-15 | 17.2 | 14.378 | 13.347 | 12.767 | L6.0 | DENIS-P J1228.2-1547 |
| 12462965-3139280 | 1246-31 | 18.2 | 15.024 | 14.186 | 13.974 | T1.0[a] | ... |
| 12545393-0122474 | 1254-01 | 18.0 | 14.891 | 14.090 | 13.837 | T2.0 | SDSSp J125453.90-012247.4 |
| 13262009-2729370 | 1326-27 | 18.6 | 15.847 | 14.741 | 13.852 | L5.0 | 2MASSW J1326201-272937 |
| 13314894-0116500 | 1331-01 | 18.4 | 15.459 | 14.475 | 14.073 | L8.5 | SDSS J133148.92-011651.4 |
| 13411160-3052505 | 1341-30 | 17.3 | 14.607 | 13.725 | 13.081 | L2.0 | 2MASS J13411160-3052505 |
| 14044948-3159330 | 1404-31 | 18.8 | 15.577 | 14.955 | 14.538 | T2.5 | 2MASS J14044941-3159329 |
| 14252798-3650229 | 1425-36 | 16.5 | 13.747 | 12.575 | 11.805 | L5.0 | DENIS-P J142527.97-365023. |

TABLE 2—*Continued*

| 2MASS ID | Red. ID | z | J | H | $K_s$ | ST | Discovery ID |
|---|---|---|---|---|---|---|---|
| 14385498-1309103 | 1438-13 | 18.2 | 15.490 | 14.504 | 13.863 | L3.0 | 2MASSW J1438549-130910 |
| 14413716-0945590 | 1441-09 | 16.4 | 14.020 | 13.190 | 12.661 | L0.5 | DENIS-P J1441-0945, G 124-6 |
| 14571496-2121477 | 1457-21 | 18.8 | 15.324 | 15.268 | 15.242 | T7.5 | Gliese 570D |
| 15074769-1627386 | 1507-16 | 15.6 | 12.830 | 11.895 | 11.312 | L5.5 | 2MASSW J1507476-162738 |
| 15200224-4422419 | 1520-44 | 16.0 | 13.228 | 12.364 | 11.894 | L4.5 | 2MASS J15200224-4422419A |
| 15230657-2347526 | 1523-23 | 17.0 | 14.203 | 13.420 | 12.903 | L2.5 | 2MASS J15230657-2347526 |
| 15302867-8145375 | 1530-81 | 17.0 | 14.154 | 13.601 | 13.404 | L0.0[b] | 2_105 |
| 15344984-2952274 | 1534-29 | 18.4 | 14.900 | 14.866 | 14.843 | T5.5 | 2MASSI J1534498-295227 |
| 15394189-0520428 | 1539-05 | 16.6 | 13.922 | 13.060 | 12.575 | L2.0 | DENIS-P J153941.96-052042. |
| 15474719-2423493 | 1547-24 | 16.3 | 13.970 | 13.271 | 12.742 | L0.0 | DENIS-P J154747.2-242349 |
| 15485834-1636018 | 1548-16 | 16.7 | 13.891 | 13.104 | 12.635 | L2.0 | 2MASS J15485834-1636018 |
| 16184503-1321297 | 1618-13 | 16.6 | 14.247 | 13.402 | 12.920 | L0.0 | 2MASS J16184503-1321297 |
| 16202614-0416315 | 1620-04 | 18.0 | 15.283 | 14.348 | 13.598 | L2.5 | GJ 618.1B |
| 16335933-0640552 | 1633-06 | 19.0 | 16.138 | 15.165 | 14.544 | L6.0 | SDSS J163359.23-064056.5 |
| 16360078-0034525 | 1636-00 | 17.0 | 14.590 | 13.904 | 13.415 | L0.0 | SDSSp J163600.79-003452.6 |
| 16452211-1319516 | 1645-13 | 15.0 | 12.451 | 11.685 | 11.145 | L1.5 | 2MASSW J1645221-131951 |
| 17054834-0516462 | 1705-05 | 16.1 | 13.309 | 12.552 | 12.032 | L4.0 | DENIS-P J170548.38-051645. |
| 17072343-0558249 | 1707-05 | 16.7 | 12.052 | 11.260 | 10.711 | L3.0 | 2MASS J17072343-0558249B |
| 17374334-1057425 | 1737-10 | 19.0 | 15.842 | 15.348 | 15.054 | T2.0[a] | ... |
| 17502484-0016151 | 1750-00 | 16.0 | 13.294 | 12.411 | 11.849 | L5.5 | 2MASS J17502484-0016151 |
| 17534518-6559559 | 1753-65 | 16.9 | 14.095 | 13.108 | 12.424 | L4.0 | 2MASS J17534518-6559559 |
| 18244550-7128196 | 1824-71 | 18.5 | 15.677 | 15.290 | 14.849 | L0.0[b] | 2_5716 |
| 18283572-4849046 | 1828-48 | 18.7 | 15.175 | 14.908 | 15.181 | T5.5 | 2MASS J18283572-4849046 |
| 18401904-5631138 | 1840-56 | 18.9 | 16.066 | 15.523 | 15.186 | L9.0[b] | 2_5580 |
| 19285196-4356256 | 1928-43 | 17.9 | 15.199 | 14.127 | 13.457 | L4.0 | 2MASS J19285196-4356256 |
| 19360187-5502322 | 1936-55 | 17.2 | 14.486 | 13.628 | 13.046 | L5.0 | 2MASS J19360187-5502322 |
| 19561542-1754252 | 1956-17 | 16.1 | 13.754 | 13.108 | 12.651 | L0.0 | 2MASS J19561542-1754252 |
| 20025073-0521524 | 2002-05 | 18.2 | 15.316 | 14.278 | 13.417 | L6.0 | 2MASS J20025073-0521524 |
| 20115649-6201127 | 2011-62 | 18.8 | 15.566 | 15.099 | 14.572 | T1.0[a] | ... |
| 20232858-5946519 | 2023-59 | 18.7 | 15.530 | 14.965 | 14.485 | T1.0[a] | ... |
| 20261584-2943124 | 2026-29 | 17.3 | 14.802 | 13.946 | 13.360 | L1.0 | 2MASS J20261584-2943124 |
| 20414283-3506442 | 2041-35 | 17.6 | 14.887 | 13.987 | 13.401 | L2.0 | 2MASS J20414283-3506442 |
| 20450238-6332066 | 2045-63 | 15.4 | 12.619 | 11.807 | 11.207 | L4.0 | SIPS2045-6332 |
| 20575409-0252302 | 2057-02 | 15.6 | 13.121 | 12.268 | 11.724 | L1.5 | 2MASSI J2057540-025230 |
| 21015233-2944050 | 2101-29 | 18.8 | 15.604 | 14.845 | 14.554 | T1.0[a] | ... |
| 21022212-6046181 | 2102-60 | 18.8 | 15.632 | 15.200 | 14.827 | T2.0[a] | ... |
| 21041491-1037369 | 2104-10 | 16.6 | 13.841 | 12.975 | 12.369 | L2.5 | 2MASSI J2104149-103736 |
| 21075409-4544064 | 2107-45 | 17.3 | 14.915 | 13.953 | 13.380 | L0.0 | 2MASS J21075409-4544064 |
| 21304464-0845205 | 2130-08 | 16.7 | 14.137 | 13.334 | 12.815 | L1.5 | 2MASSW J2130446-084520 |
| 21324898-1452544 | 2132-14 | 19.0 | 15.714 | 15.382 | 15.268 | T3.0[a] | ... |
| 21481326-6323265 | 2148-63 | 18.3 | 15.330 | 14.338 | 13.768 | L8.0[a] | ... |

TABLE 2—*Continued*

| 2MASS ID | Red. ID | z | J | H | $K_s$ | ST | Discovery ID |
|---|---|---|---|---|---|---|---|
| 21501592-7520367 | 2150-75 | 16.6 | 14.056 | 13.176 | 12.673 | L1.0 | 2MASS J21501592-7520367 |
| 21574904-5534420 | 2157-55 | 17.0 | 14.263 | 13.440 | 13.002 | L0.0 | 2MASS J21574904-5534420 |
| 21580457-1550098 | 2158-15 | 17.8 | 15.040 | 13.867 | 13.185 | L4.0 | 2MASS J21580457-1550098 |
| 22041052-5646577 | 2204-56 | 16.7 | 11.908 | 11.306 | 11.208 | T1.0 | eps Indi Ba |
| 22064498-4217208 | 2206-42 | 18.3 | 15.555 | 14.447 | 13.609 | L2.0 | 2MASSW J2206450-421721 |
| 22092183-2711329 | 2209-27 | 18.9 | 15.786 | 15.138 | 15.097 | T2,0[a] | ... |
| 22134491-2136079 | 2213-21 | 17.9 | 15.376 | 14.404 | 13.756 | L0.0 | 2MASS J22134491-2136079 |
| 22244381-0158521 | 2224-01 | 16.9 | 14.073 | 12.818 | 12.022 | L3.5 | 2MASSW J2224438-015852 |
| 22521073-1730134 | 2252-17 | 17.2 | 14.313 | 13.360 | 12.901 | L7.5 | DENIS-P J225210.73-173013. |
| 22545194-2840253 | 2254-28 | 16.5 | 14.134 | 13.432 | 12.955 | L0.5 | 2MASSI J2254519-284025 |
| 22552907-0034336 | 2255-00 | 18.0 | 15.650 | 14.756 | 14.437 | L0.0 | SDSSp J225529.09-003433.4 |
| 23101846-1759090 | 2310-17 | 16.9 | 14.376 | 13.578 | 12.969 | L1.0 | SSSPM J2310-1759 |
| 23185497-1301106 | 2318-13 | 18.8 | 15.553 | 15.237 | 15.024 | T3,0[a] | ... |
| 23302258-0347189 | 2330-03 | 17.0 | 14.475 | 13.745 | 13.121 | L1.0 | 2MASS J23302258-0347189 |
| 23440624-0733282 | 2344-07 | 17.6 | 14.802 | 13.846 | 13.232 | L4.5 | 2MASS J23440624-0733282 |
| 23462656-5928426 | 2346-59 | 17.3 | 14.515 | 13.905 | 13.500 | L5.0 | SIPS2346-5928 |
| 23515044-2537367 | 2351-25 | 14.8 | 12.471 | 11.725 | 11.269 | L0.0 | SIPS J2351-2537 |

[a]These objects have been provided pre-publication from a study being undertaken by D. Pinfield (Univ. of Hertfordshire) of the Galactic Plane. The spectral types are based on photometry.

[b]These objects have been selected from the catalog of Pokorny et al. (2004) and photometrically classified.